drones

MDPI

Article

Optimization of Multi-User Secure Communication Rate Under Swarm Warden Detection in ISAC Networks

Kuanhao Yu, Hang Hu *, Yangchao Huang, Wei Li, Weiting Gao and Guobing Cheng

College of Information and Navigation, Air Force Engineering University, Xi'an 710077, China; jzcq0519@126.com (K.Y.); gxyxhbwhyc@sohu.com (Y.H.); liweichangsha@163.com (W.L.); 13571903058@139.com (W.G.); guobingcheng12@163.com (G.C.)
* Correspondence: xd_huhang@126.com

Highlights

What are the main findings?

- We analyze the relationship between the detection error probability of swarm wardens and the communication and sensing beams within an ISAC network. Moreover, we derive the constraints that the UAV in an ISAC network can successfully conduct covert communication when the adversary employs the optimal receiver and signal-processing algorithms.
- We propose a novel approach for generating AN to maximize interference with swarm wardens while avoiding its impact on ground users.

What are the implications of the main findings?

- Our scheme takes into account the issue of covert communication under the most stringent conditions and successfully boosts the performance of covert communication, which can provide new insights for covert communication in less stringent scenarios.
- We propose a novel approach for generating AN that can maximally interfere with the adversary's receiver without affecting ground users. This approach can offer some new perspectives for the design of AN in communication systems with interference and surveillance.

Abstract

Unmanned aerial vehicle (UAV)-enabled integrated sensing and communication (ISAC) systems have been widely applied in various scenarios recently. This paper aims to maximize the total secure communication rate (SCR) of multiple users while ensuring the minimum beamforming gain towards sensing targets under the surveillance of multiple UAV warden swarms. To reduce the risk of detection, a novel type of artificial noise (AN) is introduced to interfere with swarm wardens. We conduct an analysis of the detection error probability (DEP) of these wardens and subsequently establish a mathematical model. In this model, the SCR is maximized subject to power, trajectory, sensing performance, and secure communication constraints. Since the problem is non-convex and the variables to be optimized are numerous and complex, we decompose the problem into three sub-problems. Then, an overall algorithm is proposed to solve these sub-problems separately. Simulation results demonstrate that the proposed scheme leads to a significant increase in the SCR. Moreover, the system exhibits highly stable performance in both communication and sensing tasks over time, indicating its robustness and reliability. Additionally, communication fairness among users is ensured, and energy efficiency is enhanced.

Check for updates

Academic Editor: Emmanouel T. Michailidis

Received: 23 October 2025
Revised: 2 December 2025
Accepted: 12 December 2025
Published: 1 January 2026

Copyright: © 2026 by the authors. Licensee MDPI, Basel, Switzerland. This article is an open access article distributed under the terms and conditions of the Creative Commons Attribution (CC BY) license.

Keywords: artificial noise; secure communication; swarm wardens; beamforming vectors; trajectory optimization

1. Introduction

UAV-enabled communications systems have been extensively employed in diverse scenarios owing to their flexible deployment, satisfactory channel characteristics, and the ability to serve as relay nodes [1,2]. To further improve spectrum utilization efficiency, ISAC has recently become a widely investigated research topic [3]. For instance, the integration of ISAC and space-based unmanned platforms is emerging as a critical enabler for 6G networks, addressing the requirements of the Internet of Everything (IoE) and high-precision environment awareness [4]. Furthermore, in emergency firefighting scenarios, drone swarms can be dispatched to scout the scale of the fire and perform fire-extinguishing tasks. Through mutual exchange of fire distribution information, drones in a swarm achieve real-time optimization of firefighting resource allocation [5]. Reference [6] focuses on UAV group communication applications that demand reliable media delivery and extended sky–ground line-of-sight coverage. The work pioneers research on fast and resource-efficient UAV transitions for such group communications. The proposed ETF algorithm is capable of handling diverse transition scenarios.

The non-convexity of communication beam tracking, UAV trajectory planning, and secure communication poses a significant design challenge for ISAC networks. Thus, numerous studies have comprehensively investigated numerous algorithms and technologies for this problem. Communication beam tracking effectively reduces power dissipation in unnecessary spatial directions. The authors of [7] seek to reduce the dependence on information about mobile users' locations based on space platforms while simultaneously maintaining positioning accuracy. They propose a hybrid positioning method that integrates user position obtained by satellite-based navigation signals with estimated user position through an extended Kalman filter (EKF) algorithm. The researchers of [8] integrate a novel dual-identity association (DIA)-based ISAC approach and an EKF scheme. References [7,8] both present improvements to the traditional EKF to achieve beam focusing. This approach is well-suited to dynamic scenarios. Trajectory optimization also plays a crucial role in ISAC networks. The researchers in [9] transform the optimal UAV trajectory design problem into a catenary shape determination problem. This transformation allows for flexible and continuous adjustment of UAV trajectories when user locations are uncertain. The advantage of this method lies in its adaptability to scenarios where user positions are ambiguous, and it also features low computational complexity. A dual-UAV system scheme is proposed in reference [10] to tackle the trajectory optimization and resource allocation problems by solving a series of quadratic programming problems. The paper presents a method to address the resource allocation problems in a multi-UAV system. The existing literature also includes in-depth research on secure communication. The authors of reference [11] investigate the secrecy energy efficiency problem in a scenario with a single UAV, a single user, and a single eavesdropper by employing the successive convex approximation (SCA) algorithm and Dinkelbach's scheme. Specifically, their approach falls into the category of traditional optimization algorithms for finding sub-optimal solutions. Its advantage lies in its high determinacy, but it suffers from high algorithmic complexity. Therefore, some researchers have explored algorithms that utilize machine learning for optimization. In reference [12], the authors design a long short-term memory (LSTM)-based meta-learner to predict eavesdroppers' channels. Subsequently, they develop SCA-based and zero-forcing secure precoding algorithms to maximize the sum of the SCRs.

Given that UAV-assisted communication primarily operates in open environments, ensuring transmission security in ISAC networks has emerged as a crucially important task. One approach is to perform information processing within the data packets for encrypted communication. However, this will introduce some additional communication overhead in terms of transmitted information. Another approach is to dispatch a jammer UAV to interfere with eavesdroppers [13]. Nonetheless, the additional UAV brings about extra costs and presents challenges for system optimization. In contrast to physical-layer security technologies, numerous studies focus on hiding communication signals, which offers a robust and low-system-complexity approach to secure communication. Extensive literature reviews indicate that investigations into covert communication in ISAC predominantly revolve around the following technologies: signal masking, directional communication, trajectory optimization, and power control. In [14], the authors conceal the presence of transmissions from eavesdroppers by masking the communication signal with sensing signals. In reference [15], covert communication is achieved through trajectory optimization. In reference [16], covert communication is realized via a combination of trajectory optimization, user scheduling, and power control. The authors of reference [17] propose a precoding optimization algorithm to evade warden detection. However, their algorithm, which is based on traditional optimization methods, suffers from high complexity. Thus, in [18], the researchers propose a beam optimization scheme based on Deep Graph Reinforcement Learning. In references [19,20], a method that combines beam optimization with trajectory optimization is employed to achieve covert communication. However, both papers lack a comprehensive analysis of wardens. Additionally, to address the issue of warden position detection, the authors of [21] use a method that utilizes multiple base stations to predict the wardens' real-time location.

Based on a comprehensive review of the aforementioned studies, we have identified two main issues. Firstly, there is a lack of rigorous scientific analysis regarding wardens. For example, the authors in reference [19] construct a simplistic model where the combined strength of communication and sensing signals received by the wardens should not exceed a specific threshold. Secondly, the consideration of the enemy's monitoring rigor is insufficient. Most of the previous studies primarily focus on scenarios where the wardens are on the ground or there is only one warden in the air. However, the adversary can significantly enhance detection performance by leveraging multiple distributed aerial monitors for joint detection.

By replicating the simulations of previous studies, we found that when the adversary employs more stringent surveillance methods, even with radar signal masking, the presence of sidelobes in directional communication renders the communication signals vulnerable to detection by wardens [22]. Moreover, the trajectory optimization of UAVs fails to completely evade the monitors' surveillance. Instead, it compresses the flyable area of the UAVs [15], significantly affecting the communication performance. Additionally, when both users and wardens are distributed in a scattered manner, it is challenging to apply interference without affecting the communication among users. Our research study investigates the impact of multiple aerial swarm wardens on a UAV-enabled ISAC network and introduces a novel AN scheme to boost the performance of secure communication. We combine trajectory optimization, beam optimization, and AN to achieve covert communication in the scenario where the most stringent measures are applied by wardens. The main contributions of this paper are outlined as follows:

- Comprehensive System Analysis and Modeling. We rigorously analyze the relationship between the DEP of swarm wardens and leaked signals (including communication signals, sensing signal, and AN signal) of UAVs (in the ISAC network) when a power-based detection scheme is adopted by swarm wardens. It is assumed that the

wardens adopt the most stringent measures to enhance the detection performance, which includes using the optimal criterion for DEP minimization, deploying multiple batches of UAV swarms in a distributed configuration, and equipping each UAV in the swarm with a single antenna. To ensure that the UAVs (in the ISAC network) can effectively perform sensing and communication tasks, a mathematical framework is established for dynamic beam alignment, trajectory optimization, and power allocation among communication, sensing, and AN generation. The sum of the SCRs is maximized by jointly optimizing beamforming vectors, UAV trajectory, and the AN ratio.

- Optimization of Algorithm Design. The problem of maximizing the sum of the SCRs is inherently non-convex and computationally intractable due to stringent constraints and high-dimensional beamforming vectors. To address this challenge, we decomposed the original problem into three sub-problems and solved them iteratively. We integrated the generation of the novel AN into the semidefinite programming (SDP) of the beamforming vectors, enabling the simultaneous generation of AN and communication–sensing signals. In trajectory optimization, the objective function, covert communication constraints, and minimum sensing performance constraints pose a complex non-convex problem. To tackle this challenge, we introduced auxiliary variables and adopted mathematical model approximation techniques. Through these approaches, we successfully transformed the initially intractable problem into a solvable convex optimization problem. Consequently, we effectively resolved the optimization problem of covert communication under the surveillance of multiple UAV warden swarms. Lastly, we propose an alternating optimization-based algorithm that enables the original problem to converge to an optimal solution.
- Performance Validation and Insights. Simulation results demonstrate that the proposed algorithm not only outperforms benchmark schemes in terms of achievable sum of the SCRs but also maintains consistent performance over time for communication and sensing. Specifically, it ensures fair multi-user resource allocation and eliminates the bias in the system where excessive resources are often assigned to specific users to enhance total channel capacity. Compared with the scheme without AN, our approach improves both energy efficiency and communication security.

2. System Model and Problem Formulation

2.1. Overview of the Scenario

As shown in Figure 1, in an urban scenario, under the surveillance of several swarm wardens, secure communication is conducted between a UAV and multiple legitimate users in ISAC, while a sensing task over a specified area also needs to be performed. For distinction, the UAV in the ISAC network is denoted by UAV_C, and the UAV swarm wardens are referred to as UAV_W. To increase the DEP of the wardens while avoiding interference with legitimate users, UAV_C continuously emits an AN signal that is orthogonal to the user channels.

The legitimate users are located on the ground and are denoted by the set $C = \{c_1, c_2, c_3, \ldots, c_v\}$. UAV_C conducts downlink communication with the users while simultaneously performing sensing tasks for multiple sensing targets within a specific area. The sensing targets are represented by the set $S = \{s_1, s_2, s_3, \ldots, s_w\}$.

From the wardens' perspective, to obtain satisfactory channel gain, UAV_Ws are deployed as monitors and utilize an air-to-air channel for accurate surveillance. To conduct more comprehensive surveillance in different directions, the wardens deploy multiple batches of swarms, which are positioned in designated areas to continuously monitor the transmit power of UAV_C. To enhance surveillance performance, each UAV_W within

a swarm is equipped with a single, mutually independent antenna for detection. Then, the collected data are transmitted to the swarm leader for joint processing. Since data transmission occurs within each swarm, each swarm independently determines whether communication is performed or not. The swarms are denoted by the set $J = \{j_1, j_2, j_3, \ldots, j_u\}$.

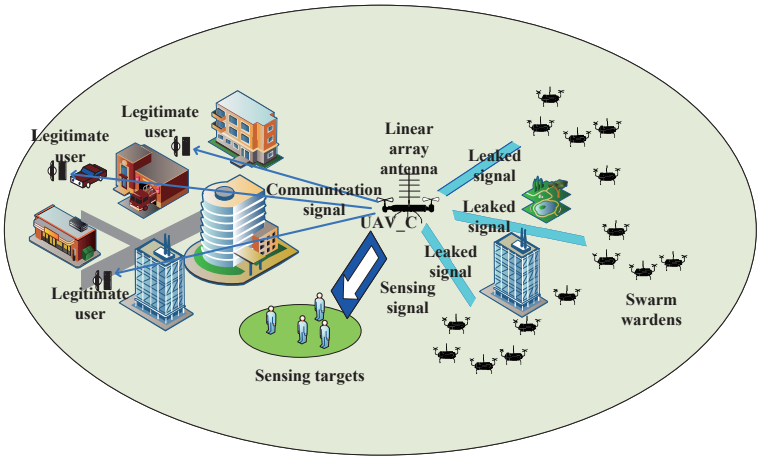


Figure 1. System model of ISAC networks.

To ensure reliable communication with legitimate users, UAV_C operates at a fixed altitude H and follows an optimal trajectory between the legitimate users and the sensing area. Fixed start and end positions are set for UAV_C. For analytical convenience, the flight time T of UAV_C is divided equally into N time slots, each with a duration of $\triangle t = \frac{T}{N}$. Each time slot is sufficiently short such that UAV_C's position can be considered unchanged [23]. The trajectory of UAV_C is defined as $Q = (x[n], y[n], H)$, where $1 \leq n \leq N$. $x[n]$denotes the x-coordinate of the communication UAV in time slot n, y$[n]$ represents the y-coordinate of the communication UAV in time slot n, and H stands for the z-coordinate (i.e., the flight altitude) of UAV_C. The speed of UAV_C is denoted by $V = (V_x[n], V_y[n])$. $V_x[n], V_y[n]$ represent the velocity components of the communication UAV's flight speed on the x-axis and y-axis, respectively.

The coordinates of legitimate users are denoted by $(x_c, y_c, 0)$, and the coordinates of sensing targets within the sensing area are represented by $(x_s, y_s, 0)$. To simplify the analysis, each swarm is treated as a single point, with the coordinates of the swarm leader representing the entire swarm. The coordinates of swarms are denoted by (x_j, y_j, H_1).

The antenna of UAV_C simultaneously emits communication signals, sensing signals, and AN. The radar signals and AN serve to mask the communication signals, while the communication signals and radar signals are jointly utilized for sensing services. This approach achieves a mutual enhancement effect between communication and sensing. The relevant analyses are as follows.

2.2. Communication Channel Model

UAV_C is equipped with an M-element linear array antenna mounted orthogonally to the horizontal plane such that the impact of UAV_C's flight orientation on the antenna radiation pattern can be avoided. And it is assumed that each legitimate user is equipped with a single antenna. These legitimate users are located in urban areas with dense high-rise buildings. Considering the need to communicate with numerous legitimate users and perform sensing tasks in a specific area, it is impossible for UAV_C to provide an LOS link for each legitimate user. Additionally, environmental factors such as reflections, scattering, and multi-path effects will have a significant impact on the channel quality between UAV_C

and users. Therefore, the UAV_C–user channel is modeled as an NLOS link, characterized by severe path loss and multi-path fading. According to [22], the channel model is

$$h_{c_i}[n] = \sqrt{\beta D_{c_i}^{-\gamma}[n]}\, a_{c_i}[n] c_i[n], \tag{1}$$

$$D_{c_i}[n] = \sqrt{(x[n] - x_{c_i})^2 + (y[n] - y_{c_i})^2 + H^2}, \tag{2}$$

where β is the channel power gain with unit distance and $D_{c_i}[n]$ is the Euclidean distance between UAV_C and the legitimate users. Parameter γ represents the path loss exponent of the UAV_C–user link. $a_{c_i}[n] \in C^{M\times 1}$ is the steering vector of the linear array antenna targeting the legitimate user. $c_i[n] \in C^{1\times 1}$ is the communication signal transmitted by UAV_C, which follows a circularly symmetric complex Gaussian (CSCG) distribution with zero mean and unit variance. The steering vector $a_{c_i}[n]$ is given as

$$a_{c_i}[n] = (1, e^{-j\frac{2\pi dH}{\lambda D_{c_i}[n]}}, e^{-2j\frac{2\pi dH}{\lambda D_{c_i}[n]}} \ldots e^{-(M-1)j\frac{2\pi dH}{\lambda D_{c_i}[n]}})^H, \tag{3}$$

where j is the imaginary unit, d is the inter-element spacing, and λ denotes the wavelength of the transmitted signal.

2.3. Analysis of Sensing Targets

Traditional sensing and communication equipment is typically deployed separately. In contrast, ISAC technology can significantly cut down hardware costs and enhance energy efficiency. Similar to the approaches in other papers, the communication and sensing signals are jointly utilized for the ISAC sensing mechanism. According to [24], to maintain the required sensing performance, UAV_C's sensing signal power must satisfy a lower-bound constraint; i.e., the radar power at the sensing target s_r must exceed a certain threshold, which is

$$\mathrm{Y}_{s_r}[n] \geq \xi D_{s_r}^2[\mathrm{n}], \tag{4}$$

where ξ denotes the minimum required gain at unit distance to achieve target detection and parameter estimation and $\mathrm{Y}_{s_r}[n]$ is the power of the joint sensing signal transmitted by the antenna, which is given as

$$\mathrm{Y}_{s_r}[n] = \left\| a_{s_r}[n] w_s[n] s[n] + a_{s_r}[n] \sum_i w_{c_i}[n] c_i[n] \right\|^2, \tag{5}$$

where $s[n] \in C^{1\times 1}$ denotes the sensing signal, $a_{s_r}[n] \in C^{M\times 1}$ is the steering vector of the linear array antenna targeting the sensing area, $w_s[n] \in C^{M\times 1}$ represents the beamforming vector of sensing signals, and $w_{c_i}[n] \in C^{M\times 1}$ represents the beamforming vector of communication signals for legitimate user c_i.

$$a_{s_r}[n] = (1, e^{-j\frac{2\pi dH}{\lambda D_{s_r}[n]}}, e^{-2j\frac{2\pi dH}{\lambda D_{s_r}[n]}} \ldots e^{-(M-1)j\frac{2\pi dH}{\lambda D_{s_r}[n]}})^H. \tag{6}$$

and

$$D_{s_r}[n] = \sqrt{(x[n] - x_{s_r})^2 + (y[n] - y_{s_r})^2 + H^2}. \tag{7}$$

x_{s_r}, y_{s_r} represent the x-coordinate and y-coordinate of sensing target s_r, respectively.

2.4. Analysis of Wardens

Each swarm consists of L members that are equipped with single, mutually independent antennas. The decision on communication activation for each swarm is determined by the received signal strength via binary hypothesis testing. Null Hypothesis (H_0): No valid

communication signal detected. Alternative Hypothesis (H_1): Valid communication signal detected. Based on [25], they are specifically expressed as follows:

$$\begin{cases} H_0 : h_{j_k}^H[n](w_s[n]s[n] + w_\sigma[n]\sigma[n]) + \sigma_j^2 \\ H_1 : h_{j_k}^H[n](w_s[n]s[n] + w_\sigma[n]\sigma[n] + \sum_{i=1}^{v} c_i[n]c_i[n]) + \sigma_j^2, \end{cases} \tag{8}$$

where $w_s[n] \in C^{M\times 1}$, $w_\sigma[n] \in C^{M\times 1}$, and $w_{c_i}[n] \in C^{M\times 1}$ denote the beamforming vectors of the sensing signals, AN signals, and communication signals which are used to steer the radiation pattern of the linear array antenna. The variable $\sigma[n]$ denotes the AN signal, and σ_j^2 is the additive white Gaussian noise (AWGN) of the wardens. Considering that the power of antenna elements can be controlled through their beamforming vectors, for convenience of analysis, we set $\|\sigma[n]\|^2 = 1$, $\|s[n]\|^2 = 1$.

Maximum ratio combining (MRC) with a phase-coherent calibration scheme is employed by swarm leaders to optimally aggregate multi-sensor signals captured by multiple winged UAV_Ws. As a result, the hypotheses presented in (8) follow a gamma distribution [26], as detailed below:

$$\begin{cases} p_0(\lambda) \sim Gamma(L, \lambda_0) \\ p_1(\lambda) \sim Gamma(L, \lambda_1), \end{cases} \tag{9}$$

$$\lambda_0 = \left\| \mathrm{h}_{j_k}^H[n](w_s[n]s[n] + w_\sigma[n]\sigma[n]) \right\|^2 + \sigma_j^2, \tag{10}$$

$$\lambda_1 = \left\| \mathrm{h}_{j_k}^H[n](w_s[n]s[n] + w_\sigma[n]\sigma[n] + \sum_{i=1}^{v} w_{c_i}[n]\mathrm{c_i}[n]) \right\|^2 + \sigma_j^2. \tag{11}$$

The probability density functions (PDFs) of the Null Hypothesis (H_0) and the Alternative Hypothesis (H_1) are

$$f(x/H_0) = \frac{x^{L-1}e^{-x/\lambda_0}}{\lambda_0^L \Gamma(L)}, \tag{12}$$

$$f(x/H_1) = \frac{x^{L-1}e^{-x/\lambda_1}}{\lambda_1^L \Gamma(L)}. \tag{13}$$

$\Gamma(L)$ is the gamma function with the independent variable L. Considering the missed detection probability and false alarm probability, the DEP for each warden swarm is denoted by

$$P_e = P(H_0)P_{FA} + P(H_1)P_{MD}. \tag{14}$$

$P(H_0)$ represents the probability of the Null Hypothesis occurring, $P(H_1)$ represents the probability of the Alternative Hypothesis occurring, P_{FA} represents the probability of false alarm, and P_{MD} represents the probability of missed detection. Referring to [27], the following inequality is satisfied by the DEP:

$$P_e \geq 1 - TVD(p_0(\lambda), p_1(\lambda)), \tag{15}$$

where TVD is the total variation distance of the distributions corresponding to the two hypotheses, which satisfies

$$TVD(p_0(\lambda), p_1(\lambda)) = \frac{1}{2}\int_{-\infty}^{\infty} |f(x|H_0) - f(x|H_1)|dx. \tag{16}$$

To ensure robust secure communication, we consider the worst-case scenario, where the wardens employ the Bayesian criterion to minimize the DEP. If the communication

remains undetectable even under such circumstances, it is certain to evade detection in other scenarios. In this case, the DEP satisfies

$$P_e = 1 - TVD(p_0(\lambda), p_1(\lambda)). \tag{17}$$

Due to the fact that the TVD is difficult to handle, Pinsker's inequality is employed to transform it into KL divergence [27].

$$TVD \leq \sqrt{\frac{1}{2} D_{KL}(p_0(\lambda) \| p_1(\lambda))}, \tag{18}$$

$$TVD \leq \sqrt{\frac{1}{2} D_{KL}(p_1(\lambda) \| p_0(\lambda))}, \tag{19}$$

where $D_{KL}(p_1 \| p_0)$ and $D_{KL}(p_0 \| p_1)$ denote the KL divergence of the distributions corresponding to the two hypotheses; they satisfy

$$D_{KL}(p_1(\lambda) \| p_0(\lambda)) = \int_{-\infty}^{\infty} f(x/H_1) \log \frac{f(x/H_1)}{f(x/H_0)} dx, \tag{20}$$

$$D_{KL}(p_0(\lambda) \| p_1(\lambda)) = \int_{-\infty}^{\infty} f(x/H_0) \log \frac{f(x/H_0)}{f(x/H_1)} dx. \tag{21}$$

To achieve the required covert communication corresponding to ε, i.e.,

$$P_{\mathrm{e}} \geq 1 - \varepsilon, \tag{22}$$

the minimum KL divergence in (20) and (21) should be selected to obtain a tighter upper bound on the TVD. With the contribution of (17)–(19), and (22), we can obtain the inequality as

$$\max[D_{KL}(p_1(\lambda) \| p_0(\lambda)), D_{KL}(p_0(\lambda) \| p_1(\lambda))] \leq 2\varepsilon^2. \tag{23}$$

Based on (12), (13), (20), (21), and (23), we can derive that

$$g(\frac{\lambda_0}{\lambda_1}) \leq \frac{2\varepsilon^2}{L}, \tag{24}$$

$$g(x) = \ln(x) + \frac{1}{x} - 1. \tag{25}$$

The detailed derivation process of Equations (24), (25) is presented in Appendix A. By substituting (10) and (11) into (24) and (25), we can obtain the constraint of covert communication, which is

$$\left\| h_{j_k}^H[n] \sum_{i=1}^{v} w_{c_i}[n] c_i[n] \right\|^2 \leq \zeta(\left\| h_{j_k}^H[n] w_s[n] s[n] + h_{j_k}^H[n] w_\sigma[n] \sigma[n] \right\|^2 + \sigma_j^2), \tag{26}$$

where ζ is the correlation coefficient, whose expression is

$$\zeta = \frac{1 - g^{-1}(\frac{2\varepsilon^2}{L})}{g^{-1}(\frac{2\varepsilon^2}{L})}. \tag{27}$$

2.5. Problem Formulation

To avoid mutual interference among users, UAV_C employs Frequency Division Multiple Access (FDMA) for communication with legitimate users. The AN signal is transmitted over a subspace channel that is orthogonal to the communication channels,

effectively preventing interference with legitimate users. According to [27], under the assumption of AWGN at all user receivers, we can derive the SCR of each user in slot n as follows:

$$R[n] = \log_2(1 + \frac{\left\|h_{c_i}^H[n]w_{c_i}[n]\right\|^2}{\sigma_c^2}). \tag{28}$$

It is assumed that prior knowledge of the swarm's member count and approximate location is accessible through adversarial reconnaissance before task execution. Subsequently, we formulate the optimization problem aiming to maximize the total communication rates of legitimate users by jointly designing UAV_C's trajectory, beamforming vectors, and AN ratio. This is subject to constraints on fixed start and end positions, energy budgets, maximum flight speed, and AN power limits. Moreover, it is required that UAV_C avoid detection by wardens (according to (26)) and meet all the sensing performance thresholds (according to (4)) for the specified targets. Consequently, the problem can be formulated as follows:

$$\max_{Q,W,\alpha} \sum_{n=1}^{N}\sum_{i=1}^{v} \log_2\left(1 + \frac{\left\|h_{c_i}^H[n]w_{c_i}[n]\right\|^2}{\sigma_c^2}\right), c_i \in \{c_1, c_2, \cdots, c_v\} \tag{29a}$$

$$\text{s.t.} \quad q[1] = q_I, \quad q[N] = q_F, \tag{29b}$$

$$|q[n] - q[n-1]| \le V_{\mathrm{m}}\Delta \mathrm{t}, n \in z^+, n \in [2, N], \tag{29c}$$

$$\|w_s[n]\|^2 + \sum_{i=1}^{v} \|w_{c_i}[n]\|^2 \le (1-\alpha)P, n \in z^+, n \in [1, N], \tag{29d}$$

$$\|w_\sigma[n]\|^2 = \alpha P, 0 < \alpha < 1, n \in z^+, n \in [1, N], \tag{29e}$$

$$\left\|a_{s_r}^H[n](w_s[n] + \sum_i w_{c_i}[n])\right\|^2 \ge \xi D_{s_r}^2(q[n]), \forall n, \forall s_r \in S, \tag{29f}$$

$$\left\|h_{j_k}^H[n]\sum_{i=1}^{v} w_{c_i}[n]\right\|^2 \le \zeta\left(\left\|h_{j_k}^H[n]w_s[n] + h_{j_k}^H[n]w_\sigma[n]\right\|^2 + \sigma_j^2\right) \tag{29g}$$

$$\forall n, \forall j_k \in J.$$

Regarding Issue (29), the following clarification is provided. Equations (29b) and (29c) represent trajectory constraints. The symbol q_I denotes the start position of the trajectory, q_F represents the end position of the trajectory, V_m is the maximum flight speed of UAV_C, and Equation (29c) represents the maximum flight speed constraint. The symbol P represents the maximum power of UAV_C in each slot, and Equations (29d) and (29e) represent power constraints; i.e., the power of the communication, sensing, and AN signals cannot exceed P in each slot, where α is the ratio of AN to total transmit power. To reduce system complexity, α is set as a time-invariant constant. Equation (29f) is the minimum sensing performance constraint, which requires that in each time slot, the sensing beam for any target within the specific area can achieve the requirement for target detection and parameter estimation. Equation (29g) is the constraint for secure communication under the surveillance of wardens, demanding that in each time slot, the communication service cannot be detected by any swarm warden.

This computationally intensive non-convex optimization problem, characterized by its high-dimensional constraints, is inherently intractable due to its combinatorial complexity. To tackle this challenge, a block coordinate descent (BCD) framework is employed to decouple the original problem into multiple interdependent sub-problems. Then, each sub-problem is reformulated by approximating it to a convex problem. Through successive iterations across blocks, updating one variable subset while fixing others, the algorithm

progressively drives the original problem to converge to an optimal solution that satisfies all the constraints.

3. Proposed Joint Optimization Algorithm

The problem involves three variables to be optimized, namely, Q, W, and α. Due to the complexity and non-convex nature of the problem, directly finding the optimal solution is extremely challenging. Using the SCA and BCD algorithms to find sub-optimal solutions proves to be a feasible approach. Therefore, the original problem is divided into three sub-problems for solution. Specifically, starting from a given initial feasible point, each sub-problem is solved iteratively by fixing the remaining variables to approach the optimal solution.

3.1. Beamforming Vector Optimization

Given feasible trajectory Q and the ratio of AN α, the beamforming vector optimization problem can be simplified as

$$\begin{aligned} &\max_{W} \sum_{n=1}^{N} \sum_{i=1}^{v} \log_2 \left(1 + \frac{\left\| h_{c_i}^H[n] w_{c_i}[n] \right\|^2}{\sigma_c^2} \right), c_i \in \{c_1, c_2, \cdots, c_v\} \\ &\text{s.t.} \quad (29d), (29e), (29f), (29g). \end{aligned} \tag{30}$$

As the communication channels vary with time slots, the AN vector should be different for each time slot. The method of generating AN at a specific time slot n is presented, and the generation methods for other time slots are the same as this one. Firstly, by performing the Householder Transformation on matrix $H_C[n] \in C^{M \times v}$ composed of user channel vectors, we obtain subspace matrix $Q_C[\mathrm{n}] \in C^{M \times (M-v)}$, which is orthogonal to any communication user channel $h_{c_i}[n] \in C^{M \times 1}$. Subspace matrix $Q_C[\mathrm{n}]$ is used to generate the AN vector, as shown in Equation (32). Then, the extreme value property of the Rayleigh quotient is employed to generate matrix $A[n]$ as shown in Equation (31), whose function is to make the projection of AN on the wardens' channels maximum. Afterward, eigenvector decomposition is performed on $A[n]$, and the eigenvector corresponding to the maximum eigenvalue is represented by $V_A[N]$. Finally, the AN vector is obtained by (32) and (33), where (33) aims to perform power normalization and make the AN vector satisfy the power constraint in Equation (29e).

$$A[n] = Q_C^H[n](H_W[n]H_W^H[n])Q_C[n],$$

$$s.t. \begin{cases} Q_C[n] \perp H_C[n] = (h_{c_1}[n], h_{c_2}[n], ..., h_{c_v}[n]), \\ Q_C^H[n] Q_C[\mathrm{n}] = I_{(M-v)\times(M-v)}, \\ H_W[n] = (h_{j_1}[n], h_{j_2}[n], ..., h_{j_u}[n]), \\ \forall n. \end{cases} \tag{31}$$

$$V_\sigma[n] = Q_C[n] V_A[N],$$

$$s.t. \begin{cases} A[n] V_A[n] = \lambda_{\max}(A[n]) V_A[n], \\ \forall n. \end{cases} \tag{32}$$

$$W_\sigma[n] = \alpha P \frac{V_\sigma[n]}{\sqrt{\|V_\sigma[n]\|^2}}, \forall n. \tag{33}$$

Given that the Signal-to-Noise Ratio (SNR) $\|h_{c_i}[n]w_{c_i}[n]\|^2/\sigma_c^2$ must exceed unity in standard communication systems, the objective function shown in (30), which can be decomposed into concave sub-functions, is also concave. But we note the non-convexity of (29f) and (29g); to address this challenge, we let

$$W_\varsigma[n] = w_\varsigma[n]w_\varsigma^H[n], \varsigma \in \{C, S\}. \tag{34}$$

Considering that time slots are independent of each other, we individually handle the beamforming vector optimization problem for each slot. Then, the semidefinite relaxation (SDR) method is employed, and the problem of (30) is transformed as follows:

$$\max_W \sum_{i=1}^{v} \log_2(1 + \frac{h_{c_i}^H[n]W_{c_i}[n]h_{c_i}[n]}{\sigma_c^2}), c_i \in \{c_1, c_2, c_3, \ldots, c_v\} \tag{35a}$$

$$\text{s.t.} \quad \text{trace}(W_s) + \sum_{i=1}^{v} \text{trace}(W_{c_i}) \leq (1-\alpha)P, \tag{35b}$$

$$a_{s_r}^H[n](W_s[n] + \sum_{i=1}^{v} W_{c_i}[n])a_{s_r}[n] \geq \xi D_{s_r}^2(q[n]), \forall s_r \in S, \tag{35c}$$

$$h_{j_k}^H[n] \sum_{i=1}^{v} W_{c_i}[n])h_{j_k}[n] \leq \zeta(h_{j_k}^H[n](W_s[n] + w_\sigma[n]w_\sigma^H[n])h_{j_k}[n] + \sigma_j^2) \quad \forall n, \forall j_k \in J, \tag{35d}$$

$$W_s[n] \succ 0, W_{c_i}[n] \succ 0, \forall c_i \in C, \tag{35e}$$

$$rank(W_s[n]) = 1, rank(W_{c_i}[n]) = 1, \forall c_i \in C. \tag{35f}$$

Through the SDR method, the left-hand sides of (29f) and (29g) are reformulated into linear functions, so constraints (29f) and (29g) become convex sets as shown in (35c) and (35d). But we observe that constraint (35f) is non-convex. Thus, the relaxation approach is adopted [28]. By disregarding constraints (35f), problem (35) is transformed into the following form:

$$\begin{aligned} &\max_W \sum_{i=1}^{v} \log_2(1 + \frac{h_{c_i}^H[n]W_{c_i}[n]h_{c_i}[n]}{\sigma_c^2}), c_i \in \{c_1, c_2, c_3, \ldots, c_v\} \\ &\text{s.t. } (35b), (35c), (35d), (35e). \end{aligned} \tag{36}$$

Problem (36) is a standard convex problem; then, we can use the CVX toolbox to solve it. Once problem (36) is solved, the Hermitian matrices $W_s[n], W_{c_i}[n], c_i \in \{c_1, c_2, c_3, \ldots, c_v\}$ are obtained. To obtain the beamforming vectors, Gaussian randomization is employed to provide an effective approximate solution to the rank-1 problem in (35).

3.2. Communication UAV Trajectory Optimization

Given beamforming vector W, the ratio of AN α, and Q_l, UAV_C trajectory optimization can be simplified as

$$\begin{aligned} &\max_Q \sum_{n=1}^{N} \sum_{i=1}^{v} \log_2\left(1 + \frac{\|h_{c_i}^H[n]w_{c_i}[n]\|^2}{\sigma_c^2}\right), c_i \in \{c_1, c_2, \ldots, c_v\} \\ &\text{s.t. } (29b), (29c), (29f), (29g). \end{aligned} \tag{37}$$

We observe that the objective function is non-concave and that constraints (29f) and (29g) are non-convex. Based on [25], two auxiliary variables are introduced as follows:

$$\ell_{\vartheta,\Theta}[n] = a_{\vartheta}^{H}[n] W_{\Theta} a_{\vartheta}[n], \vartheta \in \{S, J, C\}, \Theta \in \{S, C\}. \tag{38}$$

$$\tau_c[n] = \frac{\sigma^2{}_c}{\beta}(H^2 + \|q[n] - q_c\|^2). \tag{39}$$

For objective function (37), it can be expressed as

$$\max_{Q} \sum_{n=1}^{N} \sum_{i=1}^{v} \log_2(\ell_{c_i,c_i}[n] + \tau_{c_i}[n]) - \log_2(\tau_{c_i}[n]). \tag{40}$$

It is a non-concave function, so we can obtain its concave approximate function by the first-order Taylor expansion as follows:

$$\max_{Q} \sum_{n=1}^{N} \sum_{i=1}^{v} (R_{lc_i}[n] + R'_{c_i}[n]), \tag{41a}$$

$$R_{lc_i}[n] = \log_2(\ell_{lc_i,c_i}[n] + \tau_{lc_i}[n])$$

$$\begin{cases} \ell_{lc_i,c_i}[n] = a_{lc_i}^{H}[n] W_{c_i}[n] a_{lc_i}[n] \\ \tau_{lc_i}[n] = \frac{\sigma_c^2}{\beta}(H^2 + \|q_l[n] - q_c\|^2), \end{cases} \tag{41b}$$

$$R'_{c_i}[n] = R'_{xc_i}[n](x[n] - x_l[n]) + R'_{yc_i}[n](y[n] - y_l[n])$$

$$\begin{cases} R'_{xc_i}[n] = \frac{(\ell'_{xc_i,c_i}[n] + \tau'_{xc_i}[n]) \log_2 e}{\ell_{lc_i,c_i}[n] + \tau_{lc_i}[n]} - \frac{\tau'_{xc_i}[n] \log_2 e}{\tau_{lc_i}[n]} \\ R'_{yc_i}[n] = \frac{(\ell'_{yc_i,c_i}[n] + \tau'_{xc_i}[n]) \log_2 e}{\ell_{lc_i,c_i}[n] + \tau_{lc_i}[n]} - \frac{\tau'_{yc_i}[n] \log_2 e}{\tau_{lc_i}[n]}, \end{cases} \tag{41c}$$

where $R'_{xc_i}[n]$ and $R'_{yc_i}[n]$ denote the partial derivatives of a certain user's communication rate with respect to UAV_C's coordinates $x[n]$ and $y[n]$ in time slot n. $\ell_{lc_i,c_i}[n]$ and $\tau_{lc_i}[n]$ are the values of (38) and (39) corresponding to Q_l. The expressions for $\ell'_{xc_i,c_i}[n], \ell'_{yc_i,c_i}[n], \tau'_{xc_i}[n], \tau'_{yc_i}[n]$ in (41c) are shown as (42a), (42b), and (43).

$$\ell'_{xc_i,c_i}[n] = \sum_{m=1}^{M} \sum_{\mu=1}^{M} -\frac{j2\pi d(m-\mu)H}{\lambda D_{lc_i}^3[n]} W_{c_i}(m,\mu) e^{\frac{j2\pi d(m-\mu)H}{\lambda D_{lc_i}}} (x_l[n] - x_{c_i}), \tag{42a}$$

$$\ell'_{yc_i,c_i}[n] = \sum_{m=1}^{M} \sum_{\mu=1}^{M} -\frac{j2\pi d(m-\mu)H}{\lambda D_{lc_i}^3[n]} W_{c_i}(m,\mu) e^{\frac{j2\pi d(m-\mu)H}{\lambda D_{lc_i}}} (y_l[n] - y_{c_i}), \tag{42b}$$

where $W_{c_i}(m,\mu)$ is the element in the m-th row and μ-th column of matrix $W_{c_i}[n] = w_{c_i}[n] w_{c_i}^{H}[n]$, $w_{c_i}[n]$ is the beamforming vector obtained by beamforming vector optimization, $D_{lc_i}[n]$ is the Euclidean distance between users c_i and Q_l in time slot n, $x_l[n], y_l[n]$ represent the given initial feasible position or position obtained in the last iteration of UAV_C in time slot n, and x_{c_i} and y_{c_i} represent the X-axis and Y-axis of user c_i.

$$\begin{cases} \tau'_{xc_i}[n] = \frac{2\sigma_c^2}{\beta}(x_l[n] - x_{c_i}), \\ \tau'_{yc_i}[n] = \frac{2\sigma_c^2}{\beta}(y_l[n] - y_{c_i}). \end{cases} \tag{43}$$

By substituting (41b), (41c), (42a), (42b), and (43) into function (41a), non-concave function (40) is approximated as a linear function.

For constraint (29f), the left-hand side of the inequality is neither convex nor concave, and the right-hand side is a convex function. Consequently, the constraint does not form a convex set. The first-order Taylor expansion is performed on the left-hand side of (29f) to transform it into a linear function.

For convenience, we introduce

$$W_{\mathfrak{A}}[n] = W_{s_w}[n] + \sum_{i=1}^{v} W_{c_i,}[n] = w_s[n]w_s^H[n] + \sum_{i=1}^{v} w_{c_i,}[n]w_{c_i,}^H[n]. \tag{44}$$

By adopting this approach, constraint (29f) becomes a convex set as follows:

$$\hat{\ell}_{s_j,(c_i,s_j)}[n] \geq \xi D_{s_j}^2(q[n]), \forall n, \forall s_j \in S \tag{45}$$

where

$$\hat{\ell}_{s_j,(c_i,s_j)}[n] = \ell_{ls_j,(c_i,s_j)}[n] + \ell_{xs_j,(c_i,s_j)}[n](x[n] - x_l[n]) + \ell_{ys_j,(c_i,s_j)}[n](y[n] - y_l[n]) \tag{46}$$

For brevity, please see Appendix B for more details on (46).

For constraint (29g), neither side is convex. By transposing terms, we derive the new constraint as

$$\left\| h_{j_k}^H[n](\sum_{i=1}^{v} w_{c_i,}[n] - \zeta(w_s[n] + w_\sigma[n]) \right\|^2 \leq \zeta\sigma_j^2, \forall n, \forall j_k \in J. \tag{47}$$

We introduce

$$\begin{aligned} W_{\mathfrak{M}}[n] &= \sum_{i=1}^{v} W_{c_i,}[n] - \zeta(W_s[n] + W_\sigma[n]) \\ &= \sum_{i=1}^{v} w_{c_i,}[n]w_{c_i,}^H[n] - \zeta(w_s[n]w_s^H[n] + w_\sigma[n]w_\sigma^H[n], \end{aligned} \tag{48}$$

where $w_{c_i}[n]$, $w_s[n]$, and $w_\sigma[n]$ are beamforming vectors obtained by beamforming vector optimization. Inequality (47) is transformed into

$$h_{j_k}^H[n]W_{\mathfrak{M}}[n]h_{j_k}[n] \leq \zeta\sigma_j^2, \forall n, \forall j_k \in J. \tag{49}$$

We deploy the same method of tackling constraint (29f) in combination with the help of auxiliary variable (38). We transform (49) into

$$\ell_{j_k,(c_i,s_r)}[n] \leq \xi D_{j_k}^2[n]\sigma_j^2, \forall n, \forall j_k \in J. \tag{50}$$

Then, by applying the first-order Taylor expansion to both sides of the inequality, we can derive their convex approximations, and constraint (50) is transformed as

$$\hat{\ell}_{j_k,(c_i,s_r)}[n] \leq \frac{\xi\sigma_j^2}{\beta}\hat{D}_{j_k}[n], \forall n, \forall j_k \in J. \tag{51}$$

The detailed Taylor series expansion is expressed as follows: The left-hand side of (51) is

$$\hat{\ell}_{j_k,(c_i,s_r)}[n] = \ell_{l\,j_k,(c_i,s_r)}[n] + \ell_{x}{}'_{j_k,(c_i,s_r)}[n](x[n] - x_l[n]) \tag{52}$$

For brevity, please see Appendix C for more details on (52). The right-hand side of (51) is

$$\begin{aligned}\hat{D}_{j_k}[n] = D^2_{l_{j_k}}[n] + 2(x_l[n] - x_s)(x[n] - x_l[n]) \\ + 2(y_l[n] - y_s)(y[n] - y_l[n]),\end{aligned} \tag{53a}$$

$$D^2_{l_{j_k}}[n] = \sqrt{(x_l[n] - x_{j_k})^2 + (y_l[n] - y_{j_k})^2 + H^2}. \tag{53b}$$

To mitigate approximation errors induced by the first-order Taylor expansion and prevent the algorithm from missing the optimal solution due to oversized iteration steps, an additional constraint (54) is introduced to ensure stable algorithm performance [25]:

$$\|Q[n] - Q_l[n]\|^2 \leq Q_{\max}. \tag{54}$$

Problem (37) is transformed and presented as problem (55) through the above analysis.

$$\max_{Q} \sum_{n=1}^{N} \sum_{i=1}^{v} (R_{l\,c_i}[n] + R'_{c_i}[n]) \tag{55}$$

$$\text{s.t.} \quad (29b), (29c), (45), (51), (54).$$

Problem (55) is a standard convex problem. Therefore, we can use the CVX toolbox to solve it.

3.3. Optimization of Ratio of AN

Given beamforming vector W, UAV_C trajectory Q, and α_l derived from the last iteration or the initial setting, the optimization of the ratio of AN can be simplified as

$$\max_{Q} \sum_{n=1}^{N} \sum_{i=1}^{v} \log_2\left(1 + \frac{1-\alpha}{1-\alpha_l} \frac{h^H_{c_i}[n] w_{c_i}[n] w^H_{c_i}[n] h_{c_i}[n]}{\sigma_c^2}\right), c_i \in \{c_1, c_2, c_3, \ldots, c_v\} \tag{56a}$$

$$\text{s.t.} \quad \frac{1-\alpha}{1-\alpha_l} \left\| a^H_{s_r}[n] \left(w_{s_r}[n] + \sum_{i=1}^{v} w_{c_i}[n]\right) \right\|^2 \geq \xi D^2_{s_r}(q[n]), \forall n, \forall s_r \in S, \tag{56b}$$

$$\frac{1-\alpha}{1-\alpha_l} \left\| h^H_{j_k}[n] \left(\sum_{i=1}^{v} w_{c_i}[n] - w_s[n] - w_\sigma[n]\right) \right\|^2 \leq \zeta \sigma_j^2, \forall n, \forall j_k \in J, \tag{56c}$$

$$\left| \frac{\alpha - a_l}{\alpha_l} \right| < 0.1, \tag{56d}$$

$$0 < \alpha < 1. \tag{56e}$$

If the ratio of AN declines too rapidly after optimization, there will be no solution to the convex optimization of beamforming vectors and UAV_C's trajectory in the last iteration due to the stringent covert communication constraint. Additionally, if there is a sudden increase in the ratio of AN after optimization, the SCR tends to exhibit a sharp drop. Thus, a new constraint (56d) is introduced to ensure algorithm stability. Specifically, objective function (56a) is monotonically decreasing with respect to α, so we only need to find the minimum value of α that satisfies (56b), (56c), (56d), and (56e) for each slot. Therefore, problem (56) is a relatively simple convex problem, and we can use the CVX toolbox to solve it.

3.4. Joint Optimization Algorithm

By solving the three sub-problems, a joint optimization algorithm is given to solve problem (29). The core idea is to leverage the BCD algorithm to transform the multi-variable optimization problem into a series of single-variable optimization problems and

continuously update the variables through successive iterations. The objective function SCR will increase in each iteration. When the growth value of the SCR is lower than a certain threshold, it is considered that the algorithm has converged to a sub-optimal solution of the original problem. More details are shown in Algorithm 1.

Algorithm 1 Joint optimization algorithm for Problem (29).

1. Initialize Q_0, α_0, P. Set the number of iterations $k = 0$ and SCR $R_C = 0$.
2. **Repeat** step3-step7
3. Given $\{Q_k, \alpha_k, P\}$, solve problem (36) to obtain W_{k+1}.
4. Given $\{W_{k+1}, Q_k, Q_{\max}, \alpha_k, P\}$, solve problem (55) to obtain Q_{k+1}
5. Given $\{W_{k+1}, Q_{k+1}, \alpha_k, P\}$, solve problem (56) to obtain α_{k+1}.
6. $R_C = \frac{1}{Nv} \sum_{n=1}^{N} \sum_{i=1}^{v} \log_2(1 + \frac{\left\| h_{c_i}^H[n] w_{c_i}[n] \right\|^2}{\sigma_c^2})$
7. Update $k = k + 1$.
8. **Until** the increase of the objective function of problem (29) is below the threshold κ.

3.4.1. Analysis of Algorithm Convergence

Conclusion 1: The SCR increases after each beamforming optimization (step 3). Problem (36) aims to realign the beams after UAV_C trajectory updates. Typically, as UAV_C's trajectory continuously moves towards the users, the total SCR will increase due to the realignment of the main lobe in each iteration. However, if the updated trajectory falls into an area that is susceptible to detection by the wardens, the SCR tends to decline after step 3. But by introducing AN, this adverse situation can be avoided. Thus, the SCR increases after each beamforming optimization.

Conclusion 2: The SCR increases after each trajectory optimization (step 4). For problem (55), which aims to maximize the SCR, UAV_C's trajectory will naturally approach each user after step 4. So, the SCR increases after each trajectory optimization due to the improvement in the SNR. To ensure algorithm stability, the iteration step-size constraint is introduced in problem (55), which can further ensure that the SCR increases in each iteration after step 4.

For the entire algorithm, although AN ratio optimization in step 5 may cause a temporary decrease in the SCR, steps 3 and 4 play a dominant role in the growth of the SCR. By integrating steps 3, 4, and 5, the SCR is expected to increase in each iteration. Thus, this algorithm enables the original problem to converge to the optimal solution.

3.4.2. Analysis of Algorithm Computational Complexity

Step 3 comprises three core components: AN vector generation, convex optimization, and Gaussian randomization. AN vector generation and Gaussian randomization introduce negligible computational overhead compared with the dominant convex optimization module. Therefore, the algorithm computational complexity is determined by the convex optimization module. Referring to [29], the convex optimization module, when applied to large datasets, exhibits a computational complexity of $L_1 = l_1 N \ln(\frac{1}{\varepsilon}) O(u + w + 1 + (v+1)M^3)^{3.5}$, where ε denotes the precision of the converged solution and l_1 denotes the number of iterations of step 3. Also, the complexity of step 4 is $L_2 = l_2 \ln(\frac{1}{\varepsilon}) O(2 + N(\mathrm{v} + w + 1))^{3.5}$, where l_2 denotes the number of iterations of step 4. Given the simplicity of constraints and objective functions in AN optimization (step 5), the overall algorithm complexity is determined by step 3 and step 4: $l_1 N \ln(\frac{1}{\varepsilon}) O(u + w + 1 + (v+1)M^3)^{3.5} + l_2 \ln(\frac{1}{\varepsilon}) O(2 + N(\mathrm{v} + w + 1))^{3.5}$.

Algorithm 1 solves the original multi-variable non-convex problem by using the SCA and BCD algorithms. It is proved that the algorithm converges correctly, and its complexity primarily depends on the number of antenna elements and the flight time.

4. Numerical Results

To concretize ambiguous scenarios and evaluate the performance of the proposed algorithm, numerical simulations are conducted with the following configuration. We focus on an urban scenario where there are four communication users located at coordinates (0, 600, 0), (300, 700, 0), (650, 700, 0), (1000, 600, 0), and three sensing targets are distributed at (450, 20, 0), (500, 20, 0), (550, 20, 0). Additionally, three warden swarms, each comprising 16 members, are deployed in designated airspace with positions (0, −200, 110), (500, −150, 100), and (1000, −200, 110). All coordinates are measured in meters. Other parameter settings are given in Table 1.

Overview of results: Based on numerous simulation experiments, we find that when the most stringent measures are applied by wardens, optimizing a single variable is insufficient to achieve covert communication, especially in the absence of AN. Therefore, we focus our analysis on the scenarios where three variables and two variables are optimized. Figure 2 shows the environmental map and the optimized trajectory of UAV_C. Following Figures 3–5, the communication performance, sensing performance, and the DEP of wardens are analyzed, respectively. The discussion of Figures 6 and 7 analyzes the role of beam optimization. Figure 8 examines the balance between sensing and communication and the fairness among users. Figure 9 gives the performance analysis of different schemes. Following Figure 10, the role of trajectory optimization is analyzed. The paragraphs following Figures 10 and 11 analyze the influence of AN on trajectory and beam optimization.

Table 1. Parameter settings.

Parameter	Set Value
Flight time of UAV_C	$T = 100$ s
The inter-element spacing of liner array antenna	$d = 0.05$ m
The wavelength of the transmitted signal	$\lambda = 0.1$ m
Variance of AWGN	$\sigma_j^2 = \sigma_c^2 = -110$ dBm
Channel power gain with unit distance	$\beta = -37$ dB
Number of elements in a linear array antenna	$M = 16$
The path loss exponent	$\gamma = 3.5$
The maximum power in each slot of UAV_C	$P = 3$ dbW
Maximum flight speed of UAV_C	$V_{\mathrm{m}} = 40$ m/s
The fixed flight altitude of UAV_C	$H = 100$ m
Maximum iteration step in trajectory optimization	$Q_{\max} = 10{,}000$ m^2
Minimum required gain at unit distance for sensing	$\xi = -48$ dBw
The DEP threshold of drone swarms	$P_e = 0.005$
Number of drones in each swarm	$L = 16$
Algorithm minimum growth rate	$\kappa = 0.02$

Symbols and abbreviations in figures: 'WQA' represents 'Scheme WQA', which is the scheme proposed to maximize the SCR by the joint optimization of trajectory, beamforming vectors, and AN ratio. 'WQ' denotes 'Scheme WQ', which maximizes the SCR via the joint optimization of beamforming vectors and trajectory. 'WA' stands for 'Scheme WA', which optimizes beamforming vectors with the utilization of AN. 'QA' represents 'Scheme QA', which maximizes the SCR by jointly optimizing the trajectory and the AN ratio. In Figure 11, 'sensing' refers to the power allocated for the sensing function, abbreviated as 'sen'. Similarly, 'communication' refers to the power allocated for the communication function, abbreviated as 'comm'.

Figure 2 shows the distribution of legitimate users, sensing targets, and wardens. Red squares represent legitimate users. Green triangles represent wardens. Purple circles represent sensing targets in the specific area. According to the simulation, UAV_C initially approaches the users at the maximum speed. Subsequently, it maneuvers at slow speed to maintain stable

link quality. Finally, it returns to the end position at full speed. UAV_C continuously evades adversarial surveillance throughout the mission while jointly optimizing power allocation and trajectory to satisfy the minimum sensing performance threshold.

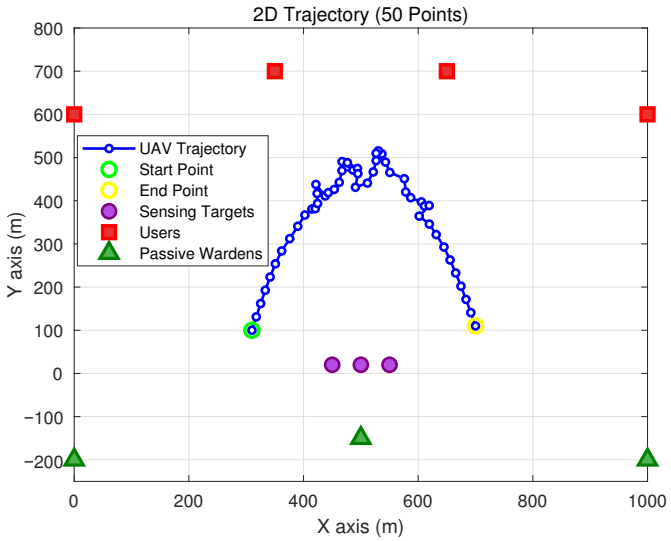


Figure 2. Environmental map and optimized trajectory of UAV_C.

Figure 3 illustrates the average SCR of four legitimate users per slot. The vertical axis represents the average communication rate of all the users. The blue line denotes Scheme 'WQA', which demonstrates superior performance. In the initial and final time slots, the SCR is comparatively low, around 2 bps/Hz. As UAV_C moves towards the users, the SCR gradually increases, reaching a maximum value of 6.41 bps/Hz. Observably, when combining trajectory optimization, beam optimization, and AN to achieve covert communication in the scenario where the most stringent measures are applied by wardens, the system performs the best. When only two of the variables are optimized, the scheme without the application of AN performs the worst.

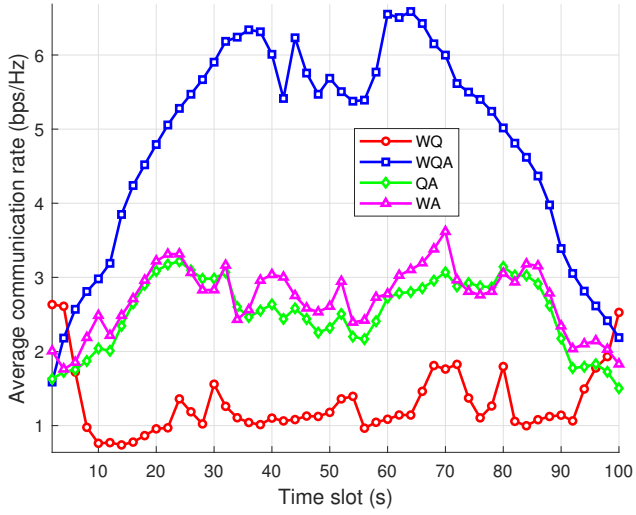


Figure 3. Average secure communication rate per slots.

Figure 4 illustrates the average sensing power of the targets in the specific area. The vertical axis represents the power reaching the sensing targets after path loss, obtained by averaging over the three targets. The blue line denotes the scheme deploying AN. According to the constraint $\xi = -48$ dBw set previously, the minimum power reaching the sensing targets is -47.2 dBw, demonstrating that the sensing performance meets the

minimum requirements across all time slots. By making a comparison with the previous figure, we can find that when the power allocated for communication is limited, the other schemes tend to allocate more power to sensing targets under the stringent constraints of the warden swarms.

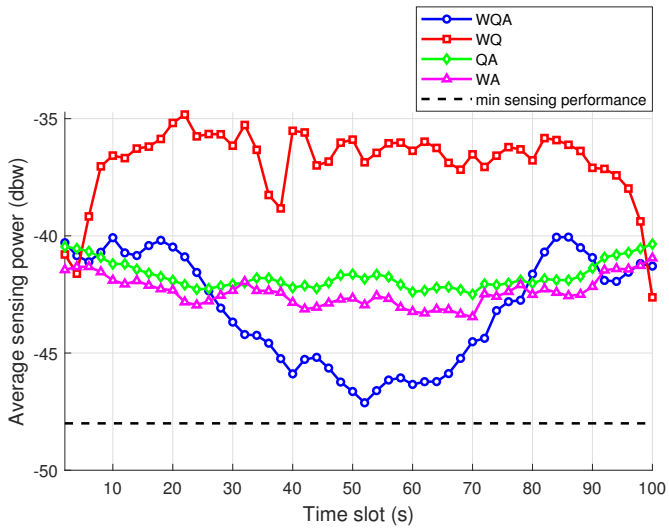


Figure 4. Sensing performance analysis.

Figure 5 depicts the DEP of three wardens in each slot. The vertical axis in each sub-plot denotes the DEP of the wardens. The three plots, arranged from top to bottom, represent the DEP corresponding to wardens 1, 2 and 3. For clarity, the DEP is converted from the linear scale to decibels (dB). The swarm wardens operate based on the relative power levels of leaked signal, which can ensure performance stability regardless of path loss. Considering the dense distribution of users, the sidelobes of communication signals are numerous and unpredictable, making it difficult to determine the strength of leaked signals in different directions. This presents a challenge to conduct a clear-cut analysis on the trend of the DEP. However, some limited analysis is possible, as presented below. Wardens 1 and 3 exhibit a similar trend in DEP due to their geometrically symmetric positions in the surveillance area. Meanwhile, warden 2, located along the central axis, demonstrates self-symmetric DEP variation over time. According to the constraint $P_e = 0.005$ set previously, the maximum DEP of the three wardens is -23 dB (i.e., 0.005), demonstrating that the covert communication performance meets the requirements across all time slots.

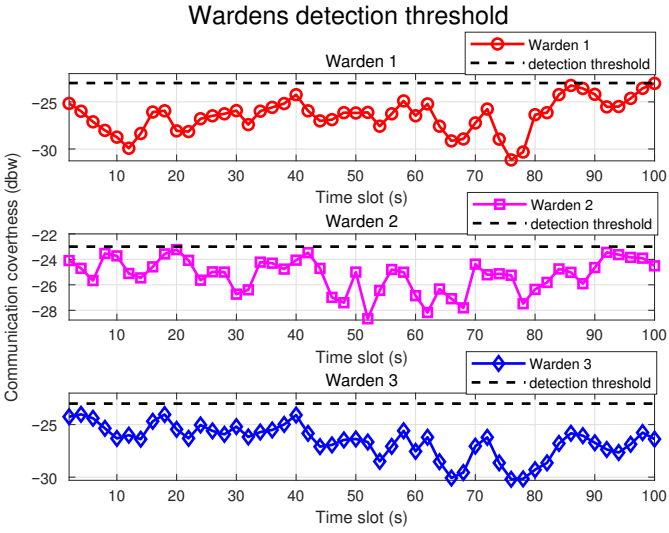


Figure 5. DEP of wardens.

Figures 6 and 7 give the azimuth and elevation radiation patterns of the linear array antenna equipped on UAV_C. The radial coordinate represents the gain of the beam, while the angular coordinate represents the orientation in the side view (Figure 6) and top view (Figure 7). The antenna radiation patterns are derived from the gain of the communication beam in different directions. Specifically, after obtaining a certain beamforming vector, we calculate the received signal power by fixing the optimized beam and varying the user positions to obtain the gain in different directions. Then, it is normalized by the reference power, which is the signal power received at the original user location. The radiation patterns exhibit high similarity across different users and time slots, with the main difference lying in the elevation angle of the main lobe. The main difference lies in the elevation angle of the main lobe. So the communication beam for user 4 in time slot 40 is selected as a representative case. As shown in Figure 7, the vertical linear array configuration of the antenna produces uniform azimuthal gain, resulting in omnidirectional beam leakage beyond the intended user direction. This inherent beam leakage allows swarm wardens to conduct surveillance. From Figure 6, we can find that UAV_C optimizes beamforming vectors to align the main radiation lobe (i.e., the lobe with a maximum gain of one) with users. Our simulation indicates that the 16-element linear array antenna achieves focused beam coverage with a 3 dB main lobe width of approximately 7.5° when the half-power beam width criterion is applied. However, sidelobes still remain in the radiation pattern. Specifically, the peak gains of the first and second sidelobes are 0.63 and 0.29, respectively, which will lead to the decrease in energy efficiency and unintended signal leakage. In summary, optimizing the beamforming vectors will improve focusing performance and substantially reduce the leakage of signals in unnecessary directions. However, when the adversary employs more rigorous surveillance techniques, the inherent limitations of linear arrays unavoidably make the communication signals easily detected by the wardens. Thus, it is of great necessity to jointly optimize the trajectory, beam, and AN.

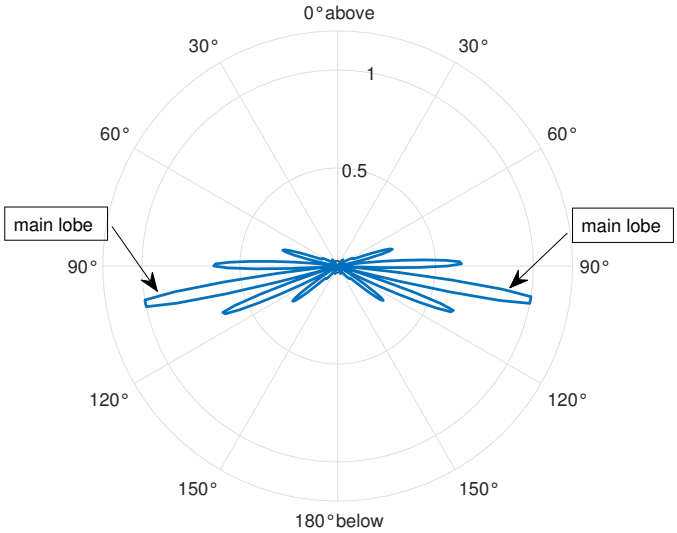


Figure 6. Elevation radiation patterns of the antenna.

Figure 8 shows the power allocation of each slot. The vertical axis denotes the power allocated to sensing beams, communication beams of users 1-4, and AN signal. Specifically, the maximum available power of UAV_C in each slot is 3 dBw, which corresponds to 2 watts. Since the ratio of AN is kept constant, its power appears as a straight line in the figure. The results demonstrate balanced power allocation between communication and sensing beams, which dynamically adapts to UAV_C's mobility to achieve optimal communication rates. The power fluctuations over time are designed to mitigate signal leakage. For instance, when the leakage of a user's communication signal toward wardens exceeds

a predefined threshold in specific time slots, UAV_C redistributes its power, reducing the communication power of this user while allocating more energy to other users. This beamforming optimization not only ensures precise beam alignment but also achieves fair power allocation among multiple users. Moreover, we observe that the presence of swarm surveillance does not force UAV_C to allocate most of the power to sensing while suppressing the power for communication to a very low level. Therefore, the proposed scheme with AN achieves good, secure communication performance.

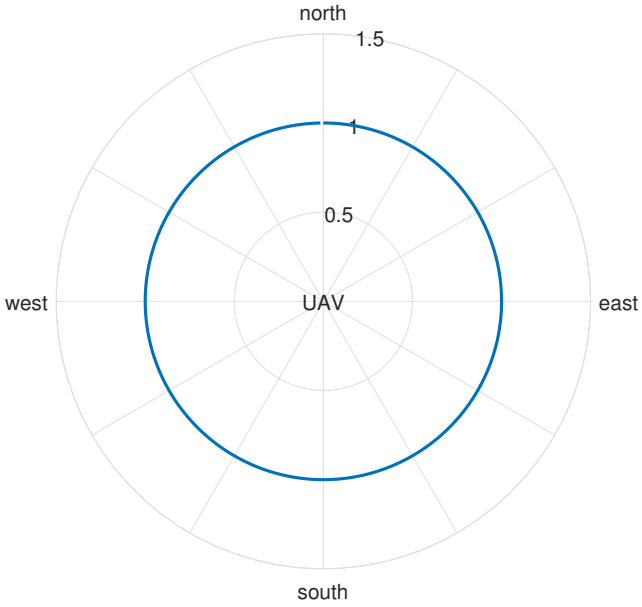


Figure 7. Azimuth radiation patterns of the antenna.

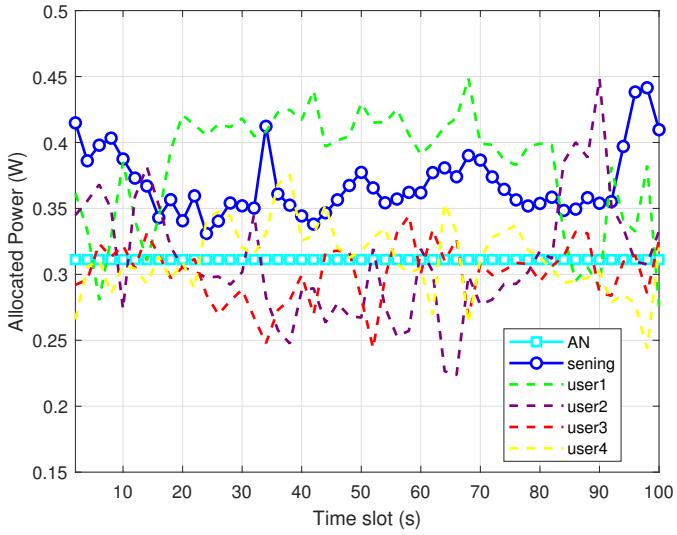


Figure 8. Power allocation.

Figure 9 illustrates the maximum achievable SCR across different communication schemes versus iteration counts, where the vertical axis represents the time-averaged and user-averaged secure communication rate. 'Scheme WQA' converges after the 11th iteration, achieving an averaged communication rate of 4.8 bps/Hz. The result of 'Scheme WQA' reveals that when AN and beam optimization are employed, the SCR attained by the random trajectory after a single iteration is approximately 3 bps/Hz. It can be concluded that the optimized trajectory exhibits a performance enhancement compared with the random trajectory. 'Scheme WQ' converges at the fourth iteration with an average rate of approximately 1.3 bps/Hz. 'Schemes WA' and 'QA' exhibit immediate convergence,

reaching rates of 2.5 and 2.4 bps/Hz, respectively. 'Scheme WQ' exhibits poor channel capacity performance due to stringent warden constraints in the AN-free scenario. 'Scheme QA' achieves limited SCR improvements since static beam misalignment occurs after optimization of UAV_C's trajectory. The underperformance of 'Scheme WA' is attributed to the fixed trajectory of UAV_C, which restricts the signal power received by the users. The proposed 'Scheme WQA' surpasses all benchmarks, demonstrating a higher SCR by jointly optimizing the ratio of AN, the beamforming vectors, and UAV_C's trajectory.

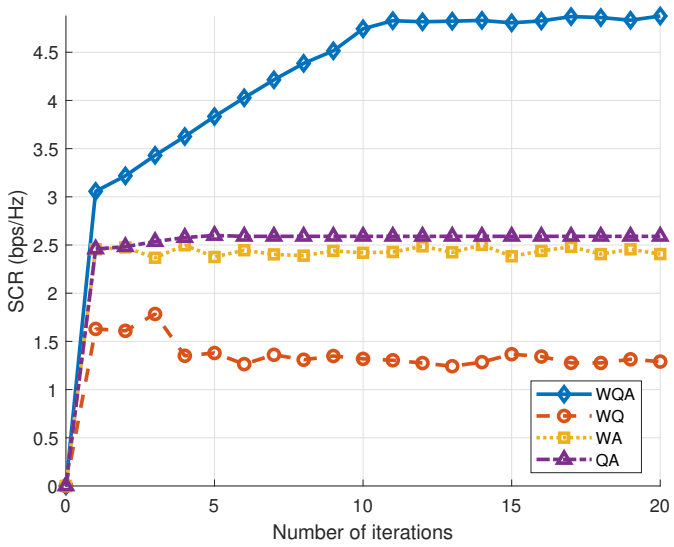


Figure 9. SCR of different schemes.

Figure 10 compares four UAV_C trajectories. 'Trajectory WQA' is the optimized trajectory of Scheme WQA. 'Trajectory WQ' is the optimized trajectory of Scheme WQ. 'Trajectory straight line' is the direct flying trajectory directly from the starting point to the destination. 'Trajectory random' is the initial trajectory Q_0 that we set randomly before optimization. From the figure, it can be observed that the optimized trajectory tends to move towards the users to enhance the channel capacities and away from the wardens for covert communication. This demonstrates the role of trajectory optimization. To illustrate the role of AN, we conduct the following analysis: When AN is employed, it provides a higher degree of freedom for the trajectory than without AN, allowing UAV_C to move as close to each user as possible. Conversely, as shown in 'Trajectory WQ', the absence of AN significantly restricts the degrees of freedom for the trajectory. Especially at $y = 300$ m, it appears that there is an obstacle restricting the trajectory, causing it to expand horizontally in a very disorganized manner. This affects the improvement in channel capacities. Therefore, introducing AN expands the feasible region for the trajectory, enabling UAV_C to provide a better service for each user. In summary, the introduction of AN can boost covert communication performance by affecting trajectory optimization.

Figure 11 analyzes the impact of the AN ratio on power allocation in three scenarios: 'zero AN injection' ($\alpha = 0$), 'optimal AN injection' ($\alpha = 0.155$), and 'excessive AN injection' ($\alpha = 0.3$). The vertical axis denotes the power allocated to sensing and communication. The figure shows that when the proportion of AN in each slot is fixed for each scheme, the sum of communication and sensing power remains fixed. First, the performance stability is analyzed as follows: Without AN, UAV_C's power allocation is subject to the stringent constraint imposed by the wardens, leading to instability. In detail, specific regions of the flight path are easily detectable, forcing UAV_C to reduce communication power to compensate for covert communication. This leads to significant fluctuations in both communication and sensing performance. Moreover, frequent power fluctuations impose

significant demands on hardware. Second, we consider the energy efficiency of different schemes. In the absence of AN, both the communication power and the sensing power are higher in the 'zero AN injection' scheme than in the other two schemes for most of the time slots. However, as analyzed in Figure 9, 'Scheme WQA' outperforms 'Scheme WQ' in terms of channel capacities. The reason is that the restricted trajectory of UAV_C, which prevents UAV_C from freely moving towards the users, leads to a consistently low level of received signal power at the user end. When the amount of AN is excessive, although UAV_C's trajectory can move towards users freely, the total power allocated to communication and sensing decreases, which in turn diminishes channel capacities. Based on the above analysis, sacrificing an appropriate proportion of power for the AN signal can enhance the stability of system performance and boost energy efficiency. In summary, the introduction of AN can boost covert communication performance by affecting power allocation, i.e., beam optimization.

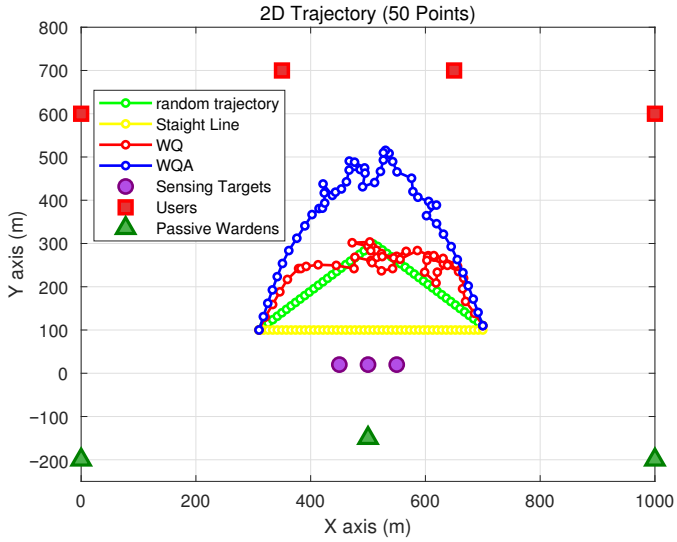


Figure 10. Influence of AN to trajectory.

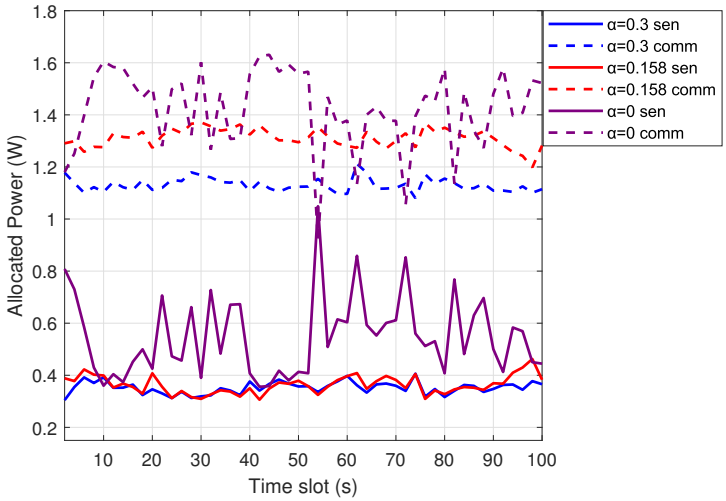


Figure 11. Influence of AN on power allocation.

5. Conclusions

This work addresses the challenge of maximizing the total SCR in a multi-user UAV-enabled ISAC system over NLOS communication channels under the surveillance of multiple adversarial wardens. We conduct a rigorous analysis of the relationship between the

DEP of warden swarms and leaked signals from the UAV in the ISAC network. And the constraint for covert communication is obtained. We assume that the wardens adopt the most stringent measures, which include using the optimal criterion for DEP minimization, deploying multiple batches of UAV swarms in a distributed configuration, and equipping each UAV in the swarm with a single antenna. To ensure communication covertness, we propose a novel approach for generating AN that can maximally interfere with the adversary's receivers without affecting ground users. In addition, an algorithm that jointly optimizes trajectory, beamforming vectors, and the ratio of AN is proposed. It is demonstrated to be an effective method. Furthermore, we conduct an in-depth analysis of the performance of the proposed scheme and examine the effects of trajectory optimization, beamforming, and AN on system performance. It is anticipated that these measures can provide new insights for covert communication in less stringent scenarios.

Author Contributions: Conceptualization, K.Y. and H.H.; Methodology, Y.H.; Software, K.Y.; Data curation, K.Y. and H.H.; Writing—original draft, K.Y.; Writing—review and editing, W.L., W.G. and G.C.; Supervision, H.H., Y.H., W.L., W.G. and G.C. All authors have read and agreed to the published version of the manuscript.

Funding: This research study was funded by Shaanxi Province Natural Science Basic Research Program (2024JC-YBMS-514) and in part by the National Natural Science Foundation of China, Grant No. 62271500).

Data Availability Statement: The original contributions presented in this study are included in this article. Further inquiries can be directed to the corresponding author.

Acknowledgments: The experimental data and some mathematical models are referenced from relevant SCI-indexed journals, and the corresponding references are provided in the reference list. We completed the simulation verification on the MATLAB R2024a platform. When writing the code, we manually built the framework and then used AI tools like Doubao and Deepseek R1 to supplement grammatical details, provide programming ideas, and correct errors. There is no other support from other institutions or organizations.

Conflicts of Interest: The funders had no role in the design of the study; in the collection, analyses, or interpretation of data; in the writing of the manuscript; or in the decision to publish the results.

Appendix A

To obtain the minimum value of the two Kullback–Leibler (KL) divergences, we first evaluate the expression in Equation (21). We substitute (12) and (13) into (21). We can obtain that

$$\begin{aligned}
D_{KL}(p_0(\lambda)\|p_1(\lambda)) &= \int_{-\infty}^{\infty} \frac{x^{L-1}e^{-x/\lambda_0}}{\lambda_0^L\Gamma(L)} \log\left(\frac{e^{-x/\lambda_0}\lambda_1^L}{e^{-x/\lambda_1}\lambda_0^L}\right)dx \\
&= \int_{-\infty}^{\infty} \frac{x^{L-1}e^{-x/\lambda_0}}{\lambda_0^L\Gamma(L)} \ln(e^{-x/\lambda_0}) - \ln(e^{-x/\lambda_1}) + \ln(\lambda_1^L)dx \\
&\quad - \ln(\lambda_0^L)dx \\
&= \int_{-\infty}^{\infty} \frac{x^{L-1}e^{-x/\lambda_0}}{\lambda_0^L\Gamma(L)}\left(\frac{-x}{\lambda_0} + \frac{x}{\lambda_1} + L\ln(\lambda_1) - L\ln(\lambda_0)\right)dx \\
&= \frac{\lambda_0^{N+1}L!}{(L-1)!\lambda_0^N}\left(\frac{1}{\lambda_1} - \frac{1}{\lambda_0}\right) \\
&\quad + \frac{\lambda_0^{N+1}(L-1)!}{(L-1)!\lambda_0^N}(L\ln(\lambda_1) - L\ln(\lambda_0)) \\
&= L\left(\ln\left(\frac{\lambda_1}{\lambda_0}\right) + \frac{\lambda_0}{\lambda_1} - 1\right)
\end{aligned}$$

and thus

$$D_{KL}(p_0(\lambda)\|p_1(\lambda)) = L(\ln(\frac{\lambda_1}{\lambda_0}) + \frac{\lambda_0}{\lambda_1} - 1). \tag{A1}$$

Similarly, we can obtain

$$D_{KL}(p_1(\lambda)\|p_0(\lambda)) = L(\ln(\frac{\lambda_0}{\lambda_1}) + \frac{\lambda_1}{\lambda_0} - 1). \tag{A2}$$

We let

$$g(x) = \ln(x) + \frac{1}{x} - 1. \tag{A3}$$

Taking the derivative of it, we get

$$g^{'}(x) = \frac{x-1}{x^2}. \tag{A4}$$

After a simple analysis, we can conclude that the function g(x) is decreasing when $x \leq 1$ and increasing when $x \geq 1$, with a steeper slope on the left-hand side of $x = 1$ than on the right-hand side. Since $\lambda_0 < \lambda_1$, we can get $\frac{\lambda_0}{\lambda_1} < 1$ and $\frac{\lambda_1}{\lambda_0} > 1$. When λ_0 and λ_1 are fixed, (A1) always lies to the left of $x = 1$, and (A2) always lies to the right of $x = 1$. Upon further analysis, we find that when λ_0 and λ_1 are fixed, (A1) is always less than (A2). So (23) is transformed into

$$D_{KL}(p_1(\lambda)\|p_0(\lambda)) \leq 2\varepsilon^2. \tag{A5}$$

$$i.e.,\ g(\frac{\lambda_0}{\lambda_1}) \leq \frac{2\varepsilon^2}{L}. \tag{A6}$$

The derivation of Equation (24) is completed.

Appendix B

Here are the details on (46):

$$\hat{\ell}_{s_j,(c_i,s_j)}[n] = \ell_{ls_j,(c_i,s_j)}[n] + \ell_{xs_j,(c_i,s_j)}[n](x[n] - x_l[n]) + \ell_{ys_j,(c_i,s_j)}[n](y[n] - y_l[n]) \tag{A7}$$

where

$$\ell_{ls_r,(c_i,s_r)}[n] = a_{ls_r}^H[n] W_{\mathfrak{A}}[n] a_{ls_r}[n], \tag{A8a}$$

$$\ell^{'}_{xs_r,(c_i,s_r)}[n] = \sum_{m=1}^{M}\sum_{\mu=1}^{M} -\frac{j2\pi d(m-\mu)H}{\lambda D_{lc_i}^3[n]} W_{\mathfrak{A}}(m,\mu) e^{\frac{j2\pi d(m-\mu)H}{\lambda D_{lc_i}[n]}} (x_l[n] - x_{s_r}), \tag{A8b}$$

$$\ell^{'}_{ys_r,(c_i,s_r)}[n]) = \sum_{m=1}^{M}\sum_{\mu=1}^{M} -\frac{j2\pi d(m-\mu)H}{\lambda D_{lc_i}^3[n]} W_{\mathfrak{A}}(m,\mu) e^{\frac{j2\pi d(m-\mu)H}{\lambda D_{lc_i}[n]}} (y_l[n] - y_{s_r}), \tag{A8c}$$

$$a_{ls_r}[n] = (1, e^{-j\frac{2\pi dH}{\lambda D_{ls_r}[n]}}, e^{-2j\frac{2\pi dH}{\lambda D_{ls_r}[n]}} ... e^{-(M-1)j\frac{2\pi dH}{\lambda D_{ls_r}[n]}})^H, \tag{A8d}$$

$W_{\mathfrak{A}}(m,\mu)$ is the element in the m-th row and μ-th column of matrix $W_{\mathfrak{A}}[n]$, $a_{ls_r}[n]$ is the steering vector of UAV_C in trajectory Q_l targeting s_r in time slot n, and $w_s[n], w_{c_i}[n]$ are the beamforming vectors obtained by beamforming vector optimization.

Appendix C

Here are the details on (52):

$$\hat{\ell}_{j_k,(c_i,s_r)}[n] = \ell_{l\,j_k,(c_i,s_r)}[n] + \ell_{x^{'}\,j_k,(c_i,s_r)}[n](x[n] - x_l[n]) + \ell_{y^{'}\,j_k,(c_i,s_r)}[n](y[n] - y_l[n]), \tag{A9}$$

where

$$\ell_{l_{j_k},(c_i,s_r)}[n] = a^H_{l_{j_k}}[n] W_{\mathfrak{M}}[n] a_{l_{j_k}}[n], \tag{A10a}$$

$$\ell'_{x_{j_k},(c_i,s_r)}[n] = \sum_{m=1}^{M}\sum_{\mu=1}^{M} -\frac{j2\pi d(m-\mu)H}{\lambda D^3_{l_{j_k}}[n]} W_{\mathfrak{M}}(m,\mu) e^{\frac{j2\pi d(m-\mu)H}{\lambda D_{l_{j_k}}[n]}} (x_l[n] - x_{j_k}), \tag{A10b}$$

$$\ell'_{y_{j_k},(c_i,s_r)}[n] = \sum_{m=1}^{M}\sum_{\mu=1}^{M} -\frac{j2\pi d(m-\mu)H}{\lambda D^3_{l_{j_k}}[n]} W_{\mathfrak{M}}(m,\mu) e^{\frac{j2\pi d(m-\mu)H}{\lambda D_{l_{j_k}}[n]}} (y_l[n] - y_{j_k}), \tag{A10c}$$

$$a_{l_{j_k}}[n] = (1, e^{-j\frac{2\pi dH}{\lambda D_{l_{j_k}}[n]}}, e^{-2j\frac{2\pi dH}{\lambda D_{l_{j_k}}[n]}} \ldots e^{-(M-1)j\frac{2\pi dH}{\lambda D_{l_{j_k}}[n]}})^H, \tag{A10d}$$

$W_{\mathfrak{M}}(m,\mu)$ is the element in the m-th row and μ-th column of matrix $W_{\mathfrak{M}}[n]$, $D_{l_{j_k}}[n]$ is the Euclidean distance between warden j_k and Q_l in time slot n, x_{j_k} and y_{j_k} represent the X-axis and Y-axis of warden j_k, and $a_{l_{j_k}}[n]$ represents the steering vector of UAV_C in trajectory Q_l targeting j_k in time slot n.

References

1. Li, H.; Xiao, M.; Wang, K.; Kim, D.I.; Debbah, M. Large Language Model Based Multi-Objective Optimization for Integrated Sensing and Communications in UAV Networks. *IEEE Wirel. Commun. Lett.* **2025**, *14*, 979–983. [CrossRef]
2. Orikumhi, L.; Bae, J.; Kim, S. Mobility-Aware Resource Allocation in UAV-Assisted ISAC Networks. In Proceedings of the 2023 14th International Conference on Information and Communication Technology Convergence (ICTC), Jeju Island, Republic of Korea, 11–13 October 2023; pp. 1042–1044.
3. Zhu, W.; Han, Y.; Wang, L.; Xu, L.; Zhang, Y.; Fei, A. Pilot Optimization for OFDM-Based ISAC Signal in Emergency IoT Networks. *IEEE Internet Things J.* **2024**, *11*, 29600–29614. [CrossRef]
4. Zhu, Q.; Liu, R.; Lv, X.; Meng, Q.; Wang, Y. AoI-Optimal Trajectory Planning in UAV-Assisted ISAC Networks. In Proceedings of the 2023 IEEE 23rd International Conference on Communication Technology (ICCT), Wuxi, China, 20–22 October 2023; pp. 428–433.
5. Luna, M.A.; Ragab, A.R.; Isac, M.S.; Peña, P.F.; Cervera, P.C. A New Algorithm Using Hybrid UAV Swarm Control System for Firefighting Dynamical Task Allocation. In Proceedings of the 2021 IEEE International Conference on Systems, Man, and Cybernetics (SMC), Melbourne, Australia, 17–21 October 2021; pp. 655–660.
6. Tu, W. Resource-efficient seamless transitions for high-performance multi-hop UAV multicasting. *Comput. Netw.* **2022**, *213*, 109051. [CrossRef]
7. Mao, W.; Lu, Y.; Pan, G.; Ai, B. UAV-Assisted Communications in SAGIN-ISAC: Mobile User Tracking and Robust Beamforming. *IEEE J. Sel. Areas Commun.* **2025**, *43*, 186–200. [CrossRef]
8. Cui, Y.; Zhang, Q.; Feng, Z.; Liu, F.; Shi, C.; Fan, J.; Zhang, P. Specific Beamforming for Multi-UAV Networks: A Dual Identity-Based ISAC Approach. In Proceedings of the ICC 2023 IEEE International Conference on Communications, Rome, Italy, 28 May–1 June 2023; pp. 4979–4985.
9. Li, Y.; Li, X.; Yang, J.; Pan, J.; Zhu, R.; Liu, H. Continuous UAV Trajectory Design with Uncertain User Location in ISAC Networks. In Proceedings of the 2024 IEEE Wireless Communications and Networking Conference (WCNC), Dubai, United Arab Emirates, 21–24 April 2024; pp. 1–6.
10. Zhang, R.; Zhang, Y.; Tang, R.; Zhao, H.; Xiao, Q.; Wang, C. A Joint UAV Trajectory, User Association, and Beamforming Design Strategy for Multi-UAV-Assisted ISAC Systems. *IEEE Internet Things J.* **2024**, *11*, 29360–29374. [CrossRef]
11. Zhao, J.; Chen, M.; Yang, Z.; Cang, Y.; Tao, Z.; Lyu, Z.; Huang, C.; Zhang, Z. Secure Resource Allocation for UAV Assisted Joint Sensing and Comunication Networks. In Proceedings of the 2022 IEEE Wireless Communications and Networking Conference (WCNC), Austin, TX, USA, 10–13 April 2022; pp. 1856–1861.
12. Al-habob, A.A.; Dobre, O.A.; Jing, Y. Predictive Beamforming Approach for Secure Integrated Sensing and Communication with Multiple Aerial Eavesdroppers. *IEEE Trans. Commun.* **2025**, *73*, 7887–7898. [CrossRef]
13. Yang, W.; Liu, X.; Liu, Z. Joint Trajectory and Resource Allocation Optimization for Mobile Vehicles in UAV Assisted Secure ISAC System. In Proceedings of the 2024 IEEE 24th International Conference on Communication Technology (ICCT), Chengdu, China, 18–20 October 2024; pp. 321–325. [CrossRef]

14. Hu, J.; Lin, Q.; Yan, S.; Zhou, X.; Chen, Y.; Shu, F. Covert transmission via integrated sensing and communication systems. *IEEE Trans. Veh. Technol.* **2024**, *73*, 4441–4446. [CrossRef]
15. Wu, J.; Yuan, W.; Hanzo, L. When UAVs Meet ISAC: Real-Time Trajectory Design for Secure Communications. *IEEE Trans. Veh. Technol.* **2023**, *72*, 16766–16771. [CrossRef]
16. Liu, Y.; Liu, X.; Liu, Z.; Yu, Y.; Jia, M.; Na, Z. Secure Rate Maximization for ISAC-UAV Assisted Communication Amidst Multiple Eavesdroppers. *IEEE Trans. Veh. Technol.* **2024**, *73*, 15843–15847. [CrossRef]
17. Al-Habob, A.A.; Dobre, O.A.; Jing, Y. Predictive Beamforming Approach for Secure Integrated Sensing and Communication. In Proceedings of the GLOBECOM 2024-2024 IEEE Global Communications Conference, Cape Town, South Africa, 8–12 December 2024; pp. 4552–4557. [CrossRef]
18. Tang, X.; Zhao, K.; Shen, C.; Du, Q.; Wang, Y.; Niyato, D. Deep Graph Reinforcement Learning for UAV-Enabled Multi-User Secure Communications. *IEEE Trans. Mob. Comput.* **2025**, *24*, 8780–8793. [CrossRef]
19. Yao, J.; Yang, Z.; Xu, J.; Quek, T.Q.S. UAV-Enabled Secure ISAC Against Dual Eavesdropping Threats: Joint Beamforming and Trajectory Design. *IEEE Wirel. Commun. Lett.* **2025**, *14*, 3199–3203. [CrossRef]
20. Yang, Z. Enhanced Security-Aware Beamforming and Trajectory Design for UAV-Assisted Integrated Sensing and Communication. In Proceedings of the 2025 5th International Conference on Sensors and Information Technology, Nanjing, China, 21–23 March 2025; pp. 710–714. [CrossRef]
21. Huang, Q.; Song, Z.; Xiong, Z.; Xu, G.; Zhao, N.; Niyato, D. Robust Sensing-Assisted Secure Communication via Cooperative Base Stations. *IEEE Trans. Commun.* **2025**, *73*, 10602–10615. [CrossRef]
22. Moon, S.; Liu, H.; Hwang, I. Joint beamforming for ris-assisted integrated sensing and secure communication in UAV networks. *J. Commun. Netw.* **2024**, *26*, 502–508. [CrossRef]
23. Zeng, Y.; Wu, Q.; Zhang, R. Accessing from the Sky: A Tutorial on UAV Communications for 5G and Beyond. *Proc. IEEE* **2019**, *107*, 2327–2375. [CrossRef]
24. Lyu, Z.; Zhu, G.; Xu, J. Joint Maneuver and Beamforming Design for UAV—Enabled Integrated Sensing and Communication. *IEEE Trans. Wirel. Commun.* **2023**, *22*, 2424–2440. [CrossRef]
25. Deng, D.; Zhou, W.; Li, X.; da Costa, D.B.; Ng, D.W.K.; Nallanathan, A. Joint Beamforming and UAV Trajectory Optimization for Covert Communications in ISAC Networks. *IEEE Trans. Wirel. Commun.* **2025**, *24*, 1016–1030. [CrossRef]
26. Chaves, D.S.; Barreto, A.N. Energy detection spectrum sensing of M-ary QAM systems over AWGN channels. In Proceedings of the 2012 International Symposium on Wireless Communication Systems (ISWCS), Paris, France, 28–31 August 2012; pp. 106–110.
27. Jia, H.; Ma, L.; Qin, D. Robust Beamforming Design for Covert Integrated Sensing and Communication in the Presence of Multiple Wardens. *IEEE Trans. Veh. Technol.* **2024**, *73*, 17135–17150. [CrossRef]
28. Si, J.; Li, Z.; Zhao, Y.; Cheng, J.; Guan, L.; Shi, J. Covert transmission assisted by intelligent reflecting surface. *IEEE Trans. Commun.* **2021**, *69*, 5394–5408. [CrossRef]
29. Sidiropoulos, D.; Davidson, T.N.; Luo, Z.-Q. Transmit beamforming for physical - layer multicasting. *IEEE Trans. Signal Process.* **2006**, *54*, 2239–2251. [CrossRef]

Disclaimer/Publisher's Note: The statements, opinions and data contained in all publications are solely those of the individual author(s) and contributor(s) and not of MDPI and/or the editor(s). MDPI and/or the editor(s) disclaim responsibility for any injury to people or property resulting from any ideas, methods, instructions or products referred to in the content.